Design of niobate nanosheet-graphene oxide composite nanofiltration membranes with improved permeability

Kunimatsu, Misato ; Nakagawa, Keizo ; Yoshioka, Tomohisa ; Shintani, Takuji ; Yasui, Tomoki ; Kamio, Eiji ; Tsang, Shik Chi Edman ; Li,…

(Citation)
Journal of Membrane Science,595:117598

(Issue Date)
2020-02-01

(Resource Type)
journal article

(Version)
Accepted Manuscript

Design of Niobate Nanosheet-Graphene Oxide Composite Nanofiltration Membranes with Improved Permeability

Misato Kunimatsu[1], Keizo Nakagawa[2]*, Tomohisa Yoshioka[1,2], Takuji Shintani[2], Tomoki Yasui[1], Eiji Kamio[1], Shik Chi Edman Tsang[3], Jianxin Li[4] and Hideto Matsuyama[1,2]*

[1]*Research Center for Membrane and Film Technology, Department of Chemical Science and Engineering, Kobe University, 1-1 Rokkodai, Nada, Kobe 657-8501, Japan.*

[2]*Research Center for Membrane and Film Technology, Graduate School of Science, Technology and Innovation, Kobe University, 1-1 Rokkodai, Nada, Kobe 657-8501, Japan.*

[3]*Department of Chemistry, University of Oxford, Oxford OX1 3QR, United Kingdom.*

[4]*State Key Laboratory of Separation Membranes and Membrane Processes, National Center for International Joint Research on Separation Membranes, School of Materials Science and Engineering, Tianjin Polytechnic University, Tianjin 300387, China.*

*Corresponding author.

Tel & Fax: +81-78-803-6302

E-mail address: knakagaw@port.kobe-u.ac.jp (K. Nakagawa)

Abstract

Membranes assembled by two-dimensional (2D) nanosheets have high potential for advanced molecular separation. The intercalation of nanomaterials into the laminar membrane is a promising strategy to control the nanochannel structure. We present 2D niobate nanosheet (NbN)-Graphene oxide (GO) composite membranes fabricated by simple vacuum filtration. The effect of the weight ratio of NbN/GO on the membrane structures and performances is investigated. The NbN-rich membranes have a more stable structure in the wet condition and a membrane structure with a larger channel size compared with GO-rich membranes. Especially, NbN55-GO45 (weight ratio of NbN/GO = 55/45) shows a superior water permeability of 20 L m^{-2} h^{-1} bar^{-1}, which is around 6 times higher than an NbN membrane (NbN100) and 2 times higher than a GO membrane (GO100), while maintaining good rejection abilities of an anionic dye (nearly 100% for Evans blue) and salt (60% for Na_2SO_4). Different models for the water pathway through nanochannels can be classified according to the composite ratio of the NbN-GO membranes.

Keywords: graphene oxide; niobate nanosheet; composite membrane; water treatment; nanofiltration

1. Introduction

The increased demand for efficient and energy saving membrane separation for water treatment has meant that the development of nanostructured materials as membranes is essential to replace the conventional polymer or inorganic membranes. Two-dimensional (2D) nanosheets have emerged as potential building blocks for membranes [1–3], because of the atomic thickness and lateral dimensions with sub micrometer to several micrometer size, large surface area, robustness and unique surface properties. The membranes fabricated using a wide variety of nanosheets, such as graphene oxide (GO) [4–15], boron nitride [16], transition metal oxides [17–19], transition metal dichalcogenides [20,21], transition metal carbides (MXene) [22], zeolites [23], metal organic frameworks (MOFs) [24] and covalent organic frameworks (COFs) [25], have been recently explored. The nanosheet membranes can be categorized according to the membrane forms, such as porous nanosheet membranes, laminar nanosheet membranes and nanosheet composite (mixed matrix) membranes [1,4]. Among them, the laminar nanosheet membranes have been extensively investigated because of the ease and variety of fabrication methods (vacuum filtration, pressure-assisted filtration, spin coating, layer-by-layer assembly, and spray coating) and the excellent molecular separation using tunable interlayer nanochannels, which can be formed through assembling each nanosheet.

GO nanosheet is an exciting building block nanomaterial for the laminar nanosheet membrane. The GO membrane has enormous potential for water treatment and desalination because of their attractive molecular sieving property with high water permeation, flexibility and surface hydrophilicity.

GO possesses hydroxyl and epoxy groups on the basal plane, carboxyl groups at the edges as well as a hydrophobic sp^2 carbon domain [26,27]. It should be noted that these functional groups are known to have a negative charge in water, which leads to the strong electrostatic repulsion for anionic species, and results in the superior rejection ability of salt and anionic dyes for the GO membrane [7,8,11,14]. However, such negatively charged surfaces cause severe swelling of GO, which significantly impairs the separation performance and may even collapse the alignment of the laminar structure [28]. To address this issue, surface reduction [29] or cross-linking [8,9] has been reported to be effective in the enhancement of the structural stability of the laminar GO membrane. However, complex and long-term surface treatment of membranes is inevitable and sometimes decreases the surface charge of GO, but also induces a decrease in the rejection ability [30].

In contrast, a transition metal oxide nanosheet could be a promising alternative to GO as a building block for functional laminar nanosheet membranes because of the attractive features such as unique surface acidity and catalytic properties. Recently, we have developed laminar metal oxide nanosheet membranes using niobate nanosheets (NbNs) [18,19]. The laminar NbN membranes exhibited an excellent stability of the structure in the wet condition through cross-linking between the acid sites on NbN and triethanolamine (TEOA). The TEOA molecules work not only as a chemical binder in the laminar nanosheet membrane, but also as a structural modifier in the bottom-up nanosheet synthesis from niobium alkoxide [31], which suggests a simple and efficient membrane fabrication approach using NbN and TEOA colloidal solution without the requirement for additional cross-linking

agents. Furthermore, the membranes showed a superior separation performance against anionic dyes and divalent anions by size exclusion and electrostatic repulsion by exploiting the negative charge of NbN. However, the precise control of the nanochannel structure in the NbN membrane is an important issue to improve the membrane performance toward application of the nanofiltration membrane (NF) because the void structure of the NbN membrane behaves as a nanochannel for water permeation.

The intercalation of nanomaterials between nanosheets is a promising strategy to control the structure of the nanochannel. Some nanomaterials, such as nanostrands, carbon dots, carbon nanotubes and 2D materials including MoS_2 and titanate nanosheets [5,10,17,32,33], have been intercalated into laminar GO membranes. For the GO/MoS_2 composite membranes, the water permeability increases upon introduction of agglomerative MoS_2 particles into the GO laminates because of the formation of a loose structure [33]. In addition, for the GO/titanate nanosheet composite membranes with ultraviolet reduction, an increased salt rejection has been observed in the filtration condition without an external hydraulic pressure [17]. Thus, it is expected that functional composite membranes with high-performance can be fabricated by assembling different kinds of 2D materials, especially metal oxide nanosheets because of their unique surface acidity and catalytic property. However, there is only one report about GO-metal oxide nanosheet composite membrane [17]. In spite of the attractive surface acidity and photocatalytic property, niobate nanosheet-based composite membrane has not been reported yet.

Therefore, in this study, we selected GO to intercalate into the laminar NbN structure to fabricate

novel NbN-GO composite membranes by simple vacuum filtration using mixed NbN and GO colloidal solutions. The effect of the weight ratio of NbN/GO on the channel structure and the membrane performance of the composite membranes is investigated.

2. Experimental

2.1. Synthesis of niobate nanosheets and graphene oxide

The NbN was synthesized by hydrothermal synthesis according to our previous study [31]. In a typical experiment, niobium (V) ethoxide (Kojundo Chemical Laboratory Co., Ltd., Saitama, Japan, 1.989 g) was mixed with TEOA (3.735 g). The solution was stable against hydrolysis and the condensation reaction at room temperature because of the chelating effect of TEOA. Then the solution was added to a 28% NH_3 aqueous solution (25 mL). The mixture (pH = 12.8) was transferred to a Teflon autoclave with a capacity of 45 mL and aged at 160 °C for 24 h. After centrifugation (6000 rpm, 10 min), the supernatant colloid was collected as NbN.

The GO nanosheet was synthesized by an improved Hummers' method according to the previous reports [34,35]. In a typical experiment, graphite (3.0 g) and $KMnO_4$ (18.0 g) were mixed with a solution of concentrated H_2SO_4 (360 mL) and H_3PO_4 (40 mL). After stirring at 50 °C for 12 h, the mixture was then poured onto ice (400 mL) and mixed with 30% H_2O_2 (3 mL). The mixed solution was further stirred for 30 min and then centrifugation (3500 rpm, 5 min) was performed to remove the precipitates. The suspension was centrifuged (6000 rpm, 20 min) and the supernatant was decanted.

Finally, the GO aqueous dispersion was obtained by successive washing with water (200 mL), 30% HCl (200 mL) and ethanol (200 mL).

2.2. Fabrication of NbN membrane, GO membrane and NbN-GO composite membranes

Laminar nanosheet composite membranes were fabricated by a simple vacuum filtration using a NbN and GO nanosheet colloidal solution. The porous mixed cellulose nitrate (CN; Merck KGaA, Darmstadt, Germany, pore size: 50 nm) was used as a support. The CN support was modified by 3-aminopropyl-triethoxysilane (APTES; Shin-Etsu Chemical Co., Tokyo, Japan) [18]. Vacuum filtration of the NbN and GO nanosheet solution was performed to form a nanosheet composite membranes on the support. The total amount of nanosheets for all membranes was controlled to be 0.14 mg. The NbN and GO membranes were fabricated according to the previous reports [18,36]. Typically, a 2.8 mg L^{-1} NbN colloidal solution (50 mL) including TEOA was used to fabricate the NbN membrane. For the fabrication of the GO membrane, TEOA was added to the GO colloidal solution as a cross-linker to improve the structural stability. The weight ratio of TEOA to GO was adjusted to 0.5. A 2.8 mg L^{-1} GO colloidal solution (50 mL) was used. These two colloidal solutions yielded laminar nanosheet membranes with a thickness of approximately 45–60 nm. The obtained membranes were dried using vacuum filtration for 2 h to remove water in the membrane and strengthen the adhesion between each nanosheet. The obtained membranes are herein denoted as NbN100 and GO100. For the fabrication of the NbN-GO composite membrane, mixed NbN and GO colloidal solutions with different weight ratios

of NbN/GO (90/10, 55/45 and 25/75 wt%/wt%) were used. The concentration of the mixed solution was adjusted to 2.8 mg L^{-1} by adding Milli-Q water. The fabrication method for the composite membranes was the same as that for the NbN and GO membranes. The obtained membranes are herein denoted as NbN90-GO10, NbN55-GO45 and NbN25-GO75.

2.3. Characterization

To obtain electron microscopy images of the nanosheet samples, transmission electron microscopy (TEM; JEM-2100F, JEOL Ltd., Tokyo, Japan) and field emission scanning electron microscopy (FE-SEM; JSF-7500F, JEOL Ltd.) were performed. Laminar structure of the membrane was measured using X-ray diffraction (XRD; RINT 2500 VHF, Rigaku Corp., Tokyo, Japan). The measurement of XRD was performed using monochromatized Cu Kα radiation (measurement condition: 40 kV and 40 mA). The surface chemical state of the membrane was measured by X-ray photoelectron spectroscopy (XPS; JPS-9200, JEOL Ltd.). The ζ-potential of the sample surfaces was analyzed using electrophoretic light-scattering (ELSZ-1000, Photal Otsuka Electronics, Osaka, Japan) in aqueous Na_2SO_4 solution (500 ppm, pH = 7.0).

2.4. Evaluation of membrane performance

A cross-flow membrane filtration system was employed for the evaluation of the membrane performances according to the previous report [18]. The effective membrane area was 7.07×10^{-4} m^2.

The applied pressure was 4 bar and the flow rate of feed water was 1.0 mL min^{-1}. To exclude concentration polarization, the feed solution side of the membrane cell was stirred. The values of water permeability were estimated from the mass changes of permeate.

Polyethylene glycol (PEG; Sigma-Aldrich Corp., St. Louis, MO, USA), with an initial concentration of 1.0 g L^{-1}, with different molecular weights (Mw) was used for the estimation of the membrane rejection performance. A total organic carbon analyzer (TOC-VCSH; Shimadzu Co., Kyoto, Japan) was used for the measurement of the PEG concentration. The rejection performance of salts (NaCl and Na_2SO_4) and the anionic dye Evans blue (EB; Mw: 960.8) was also investigated. An NaCl and Na_2SO_4 solution (500 ppm each) was used as the feed solution and concentrations were measured with a sodium ion meter (LAQUA twin B-722; HORIBA, Ltd., Kyoto, Japan). An EB aqueous solution (10 ppm) was used as the feed solution. The concentration of EB was measured from the absorbance (λ = 609 nm) using a UV/Vis spectrophotometer (V-650, JASCO International Co., Ltd., Tokyo, Japan). The rejection of solute was calculated by the following equation: R (%) = $(1 - C_P/C_F) \times 100$. The C_F and C_P are the concentrations of the feed and the permeate solutions, and R is the rejection.

3. Results and discussion

3.1 Fabrication and characterization of nanosheet composite membranes

The NbN was synthesized by the hydrothermal method using niobium (V) ethoxide with a chelate reagent of TEOA. Another nanosheet of GO was synthesized by the improved Hummer's method using

graphite as a carbon source. The NbN membrane, GO membrane and NbN-GO composite membranes were assembled by a simple vacuum filtration. The structural analysis of these composite membranes was performed using TEM, FE-SEM, XRD and XPS.

Fig.1 shows the TEM images of the NbN and GO. Many distinct flat and sharp edged sheets with a lateral size of around 40–200 nm were observed for NbN (Fig. 1a), whereas the exfoliated GO nanosheet with a lateral size of 3–6 μm was observed (Fig. 1b). The oxidation degree of GO was analyzed using XPS (Fig. S1 and Table S1 in Supplementary Information (SI)). The whole spectrum could be divided into four peaks [27]. A main peak at 284.0 eV was associated with C-C bonding, which corresponded to the sp^2 carbon in graphene regions and the area ratio (AR) of this peak was 51.0%. The peak at 286.1 eV was related to C-O bonding in both the epoxy and hydroxyl groups and AR was 37.7%. Another two peaks (287.1 and 288.0 eV) corresponded to C=O bonding of carbonyl groups and O-C=O bonding of carboxylic groups and the AR were 6.1 and 5.1%, respectively. Therefore the oxidation degree was estimated to 49.0%.

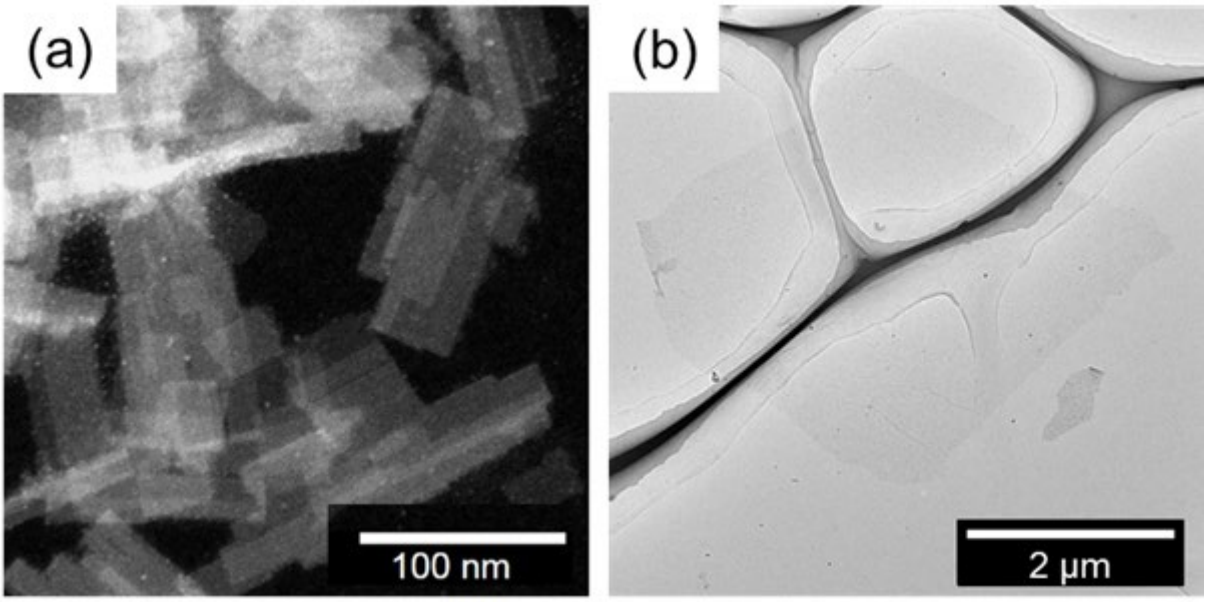

Fig. 1 (a) STEM image of NbN and (b) TEM image of GO.

The SEM images of the top view and cross-section for the NbN membrane, GO membrane and NbN-GO composite membranes with different composite ratios are shown in Figs 2 and 3. Small nanosheets with a lateral size of a few hundred nanometers seemed to stack on the surface for NbN100 (Fig. 2a), whereas rough surfaces with many wrinkles, which are peculiar for graphene with a flexible structure, were observed for GO100 (Fig. 2e). The NbN90-GO10 had a similar surface aspect as NbN100. Some wrinkles were observed on the membrane surface with a higher weight ratio of GO, such as for NbN55-GO45 and NbN25-GO75. When viewed in the cross-section, thin layers with a similar thickness of around 45–60 nm in average were observed on the support for all membranes (Fig.3). However, the thickness of the composite membranes with a higher weight ratio of GO were slightly thicker in spite of the same amount of nanosheets on the support for all membranes. For example, a thicker membrane formed for NbN55-GO45 (average thickness: 55 nm) as compared with NbN100 (average thickness: 45 nm). This resulted from the formation of a membrane structure with

high porosity for NbN55-GO45, as will be discussed below.

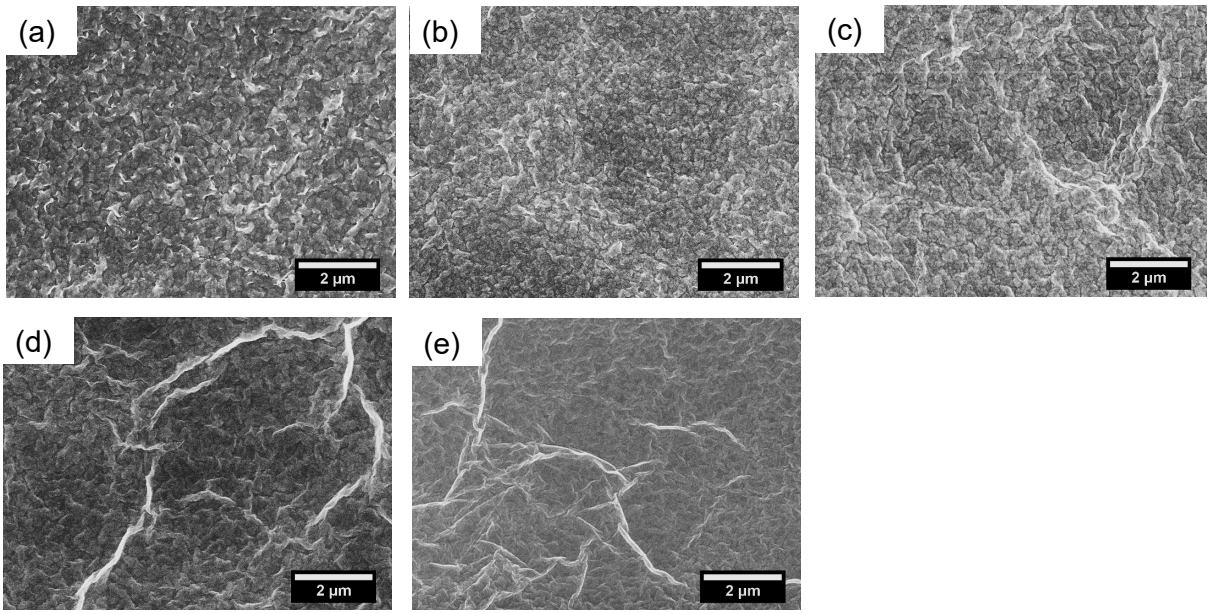

Fig. 2 Top view SEM images of (a) NbN100, (b) NbN90-GO10, (c) NbN55-GO45, (d) NbN25-GO75 and (e) GO100.

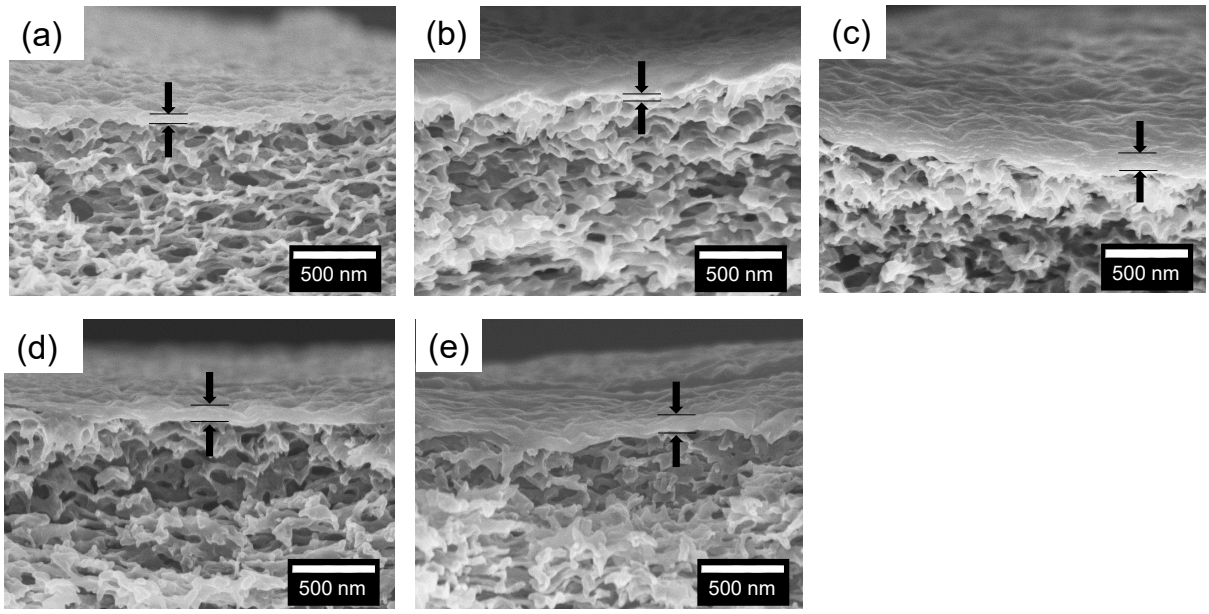

Fig. 3 Cross-sectional SEM images of (a) NbN100, (b) NbN90-GO10, (c) NbN55-GO45, (d) NbN25-GO75 and (e) GO100.

The cross-sectional STEM images and elemental mappings for NbN100 and NbN55-GO45 were also observed (Fig. 4). The formation of a thin layer with a thickness of 20–30 nm, which exhibited a

high contrast on a porous material, was clearly confirmed, as shown in Fig. 4a. From the analysis of elemental mapping, the signals of niobium were detected at the thin layer (Fig. 4b). This result indicated that a thin layer of laminar niobate nanosheets was formed on the surface of the porous cellulose nitrate support. The difference in the membrane thickness estimated by SEM and STEM implies the existence of the partial thickness unevenness. For the measurement of NbN55-GO45, a thin membrane composed of layer-like contrast was observed, as shown in Fig. 4c. Such a layer-like contrast resulted from the difference of electron density between Nb and C. From the analysis of elemental mapping, signals of niobium were clearly detected in the parts of the thin layer (Fig. 4d). These results implied that NbN and GO were stacked by the mixture on the support for NbN55-GO45.

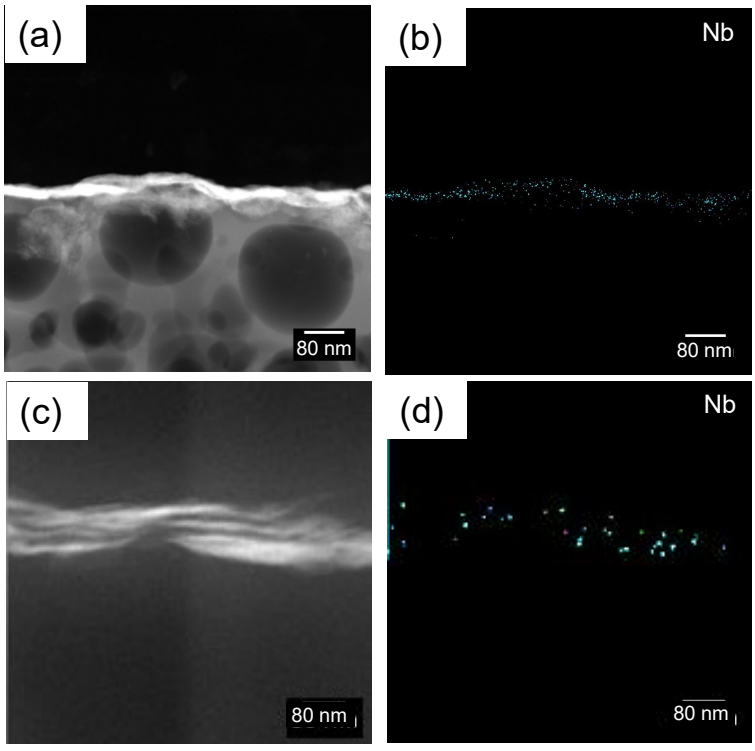

Fig. 4 Cross-sectional STEM images (a, c) and EDS elemental mapping of niobium (Nb) (b, d) for NbN100 (a, b) and NbN55-GO45 (c, d).

Fig. 5 shows the XRD patterns of NbN100, NbN-GO composite membranes and GO100 in dry and wet conditions. The diffraction peaks attributed to the interlayer spacing (*d*-spacing) for all membranes were observed in both conditions. The values of the *d*-spacing calculated using Bragg's low for each membrane are listed in Table 1. In the dry condition (black lines), the diffraction peaks of NbN100 and NbN-GO composite membranes were observed at lower angles than that of GO100, although the diffraction peak of NbN25-GO75 was very broad. In the wet condition (red lines), the peaks of all membranes were found to shift toward a lower angle compared with the peaks in dry condition. The values Δd shown in Table 1 are the difference of the *d*-spacing between dry and wet conditions. It should be noted that the degree of peak shifts for NbN100, NbN90-GO10 and NbN55-GO45 was very small (0.1 nm), whereas that of GO100 was larger (0.6 nm) and that of NbN25-GO75 was also relatively large (0.3 nm). Thus, these results suggested that NbN100, NbN90-GO10 and NbN55-GO45 have a potential to retain a highly stable structure in wet conditions as compared with NbN25-GO75 and GO100.

Such an enlargement of the interlayer distance for GO100 implied a swelling of the laminar structure in the wet condition. It should be noted that water molecules could diffuse into the interlayer spacing because of the highly hydrophilic surface of GO nanosheets, even though the GO layers were cross-linked by multivalent cations and chemical binders [8,9] or the surface of GO was partially reduced [29], which induced the swelling phenomenon [28,37]. However, only a slight increase in the interlayer distance was observed for NbN100, NbN90-GO10 and NbN55-GO45. In a previous study,

we reported that niobate nanosheet membranes (NbN100 in this study) showed an excellent stability of the structure in the wet condition through cross-linking with the help of the chemical binders APTES and TEOA [18]. The coordination and hydrogen bonding between surface acid sites (Brønsted and Lewis acid sites) on the niobate nanosheets [38,39] and chemical binders of amine molecules enabled the formation of the dense and stable structure. Furthermore, we reported that the structural stability of GO membranes (GO100 in this study) was improved by the addition of TEOA [36]. An electrostatic interaction between N^+ groups of TEOA and GO carboxyl groups and hydrogen bonding between hydroxyl groups of TEOA enhanced the structural stability. Thus TEOA would serve as a bridge between NbN and GO nanosheets for NbN-GO composite membranes.

Based on the structural stability of NbN100 and GO100, the structures of NbN-GO composite membranes were considered. The number and volume of NbN and GO layers of each membrane could be estimated by considering the amount of NbN and GO layers on the support, average sheet area, thickness of monolayer and density, as listed in Table S2. The number of NbN layer was five orders of magnitude larger than that of GO for NbN90-GO10 and three orders of magnitude larger than that of GO for NbN55-GO45 and NbN25-GO75 because of the large difference of the average sheet size and density between the NbN and GO layers. With regards to the volume, as expected, the volume of the NbN layer was 3.8 times larger than that of the GO layer for NbN90-GO10 and, conversely, the volume of the GO layer was 7.1 times larger than that of the NbN layer for NbN25-GO75. These estimations and the XRD results could be associated with the composite structure, where a small number and

volume of GO layers were set up in places in the membranes composed of a large majority of NbN layers for NbN90-GO10 (NbN-based channel structure), and the opposite situation for the composite structure could be applicable for NbN25-GO75 (GO-based channel structure). However, it was found that the volume of the GO layer was slightly larger than that of the NbN layer for NbN55-GO45 even though the weight of each sheet was similar. Considering the results of only a slight peak shift in XRD (which suggested a stable structure) and the estimation of the nanosheet volume, the structure of NbN55-GO45 was applied in the transition region between the NbN-based channel structure and GO-based channel structure. The details of the membrane structure will be discussed later.

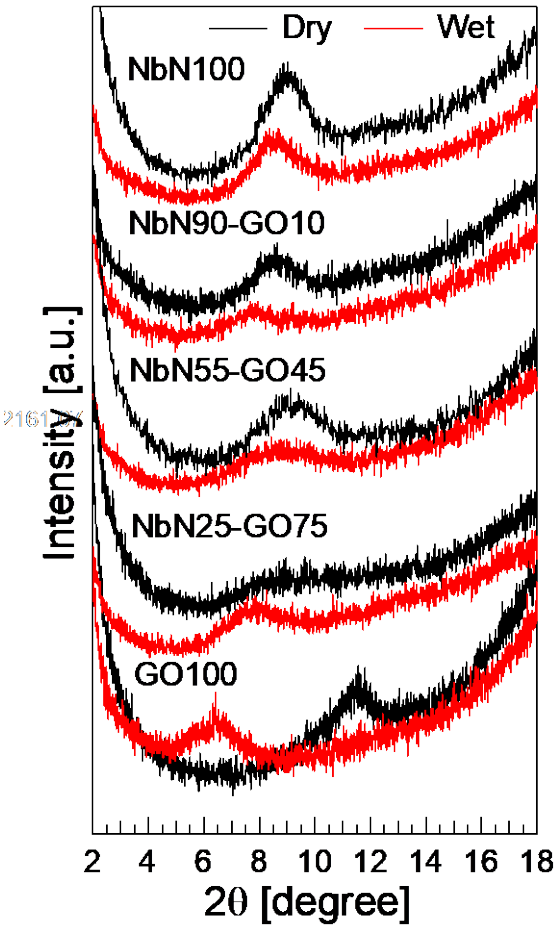

Fig. 5 XRD patterns of NbN100, NbN-GO composite membranes and GO100 in dry and wet conditions. The membrane thickness was around 100 nm.

Table 1. Values of *d*-spacings and Δ*d* for NbN100, NbN-GO composite membranes and GO100.

Membranes	*d* (dry) [nm]	*d* (wet) [nm]	Δ*d* [nm]
NbN100	1.0	1.1	0.1
NbN90-GO10	1.0	1.1	0.1
NbN55-GO45	0.9	1.0	0.1
NbN25-GO75	0.9	1.2	0.3
GO100	0.8	1.4	0.6

3.2 Membrane performance of nanosheet composite membranes

The membrane performances for the nanosheet composite membranes with a thickness of around 45–60 nm in average were measured. Fig. 6 shows the water permeability of NbN100, NbN-GO composite membranes and GO100. Interestingly, all NbN-GO composite membranes showed a higher water permeability than NbN100. Especially, NbN55-GO45 showed a water permeability of 20 L m^{-2} h^{-1} bar^{-1}, which was around 6 times higher than NbN100 and 2 times higher than GO100. Thus, the water permeability of NbN100 was apparently improved by the addition of GO.

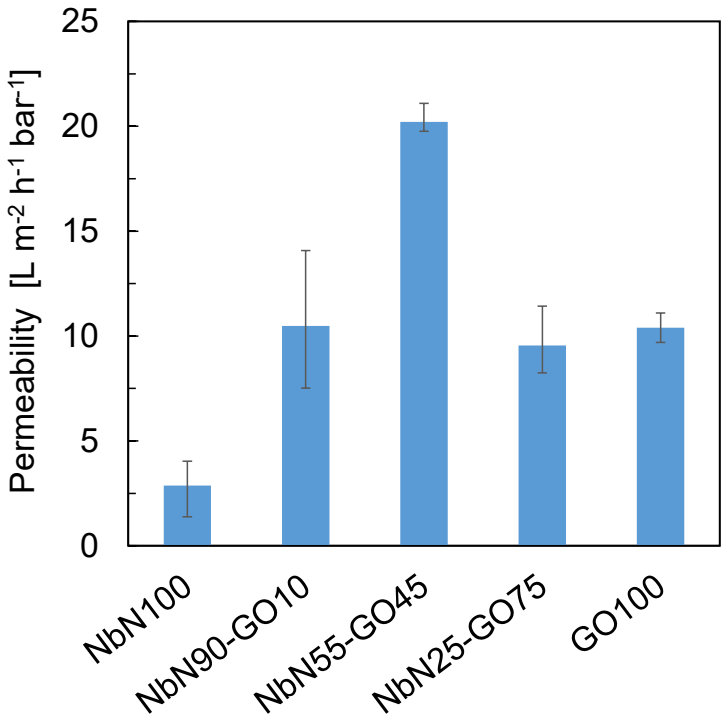

Fig. 6 Water permeability of NbN100, NbN-GO composite membranes and GO100.

The curves of the molecular weight cutoffs (MWCOs) for each membrane using PEG with a range of molecular weight are shown in Fig.7. The values of MWCO were estimated at the molecular weight at which 90% rejection was achieved [32]. Whilst some errors in the estimation of rejection still exist,

the GO-rich membranes (GO100 and NbN25-GO75) had a relatively small MWCO of around 2000 whereas the NbN-rich membranes (NbN100, NbN90-GO10 and NbN55-GO45) had a large MWCO of over 4000. A correlation between molecular weight of PEG and the Stokes-Einstein radius estimated from the viscosity measurement has been previously reported [40] :

$$\text{Solute radius (nm)} = (0.262 \times M_w^{0.5} - 0.3) \times 0.1$$

The values of the MWCOs and the estimated solute diameters are listed in Table 2. It was interesting to observe that there was a difference in the estimated sizes of the nanochannels between NbN-rich membranes and GO-rich membranes: NbN-rich membranes had larger nanochannels (3.3 nm for NbN100, 4.0 nm for NbN90-GO10 and 4.6 nm for NbN55-GO45) as compared with GO-rich membranes (2.4 nm for NbN25-GO75 and 2.3 nm for GO100).

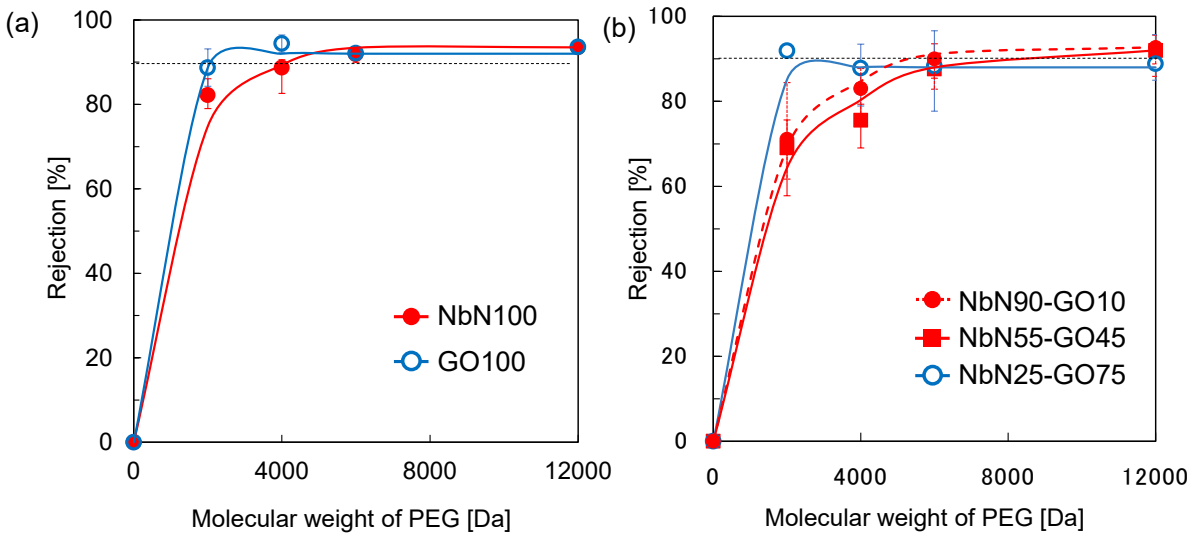

Fig. 7 MWCO using PEG for (a) NbN100 and GO100 and (b) NbN-GO composite membranes.

Table 2. Molecular weight cutoffs (MWCOs) measured using PEG, calculated solute diameters and surface ζ-potential at pH = 7.0 for NbN100, NbN-GO composite membranes and GO100.

Membranes	MWCO [Da]	Solute diameter [nm]	ζ-potential [mV]
NbN100	4200	3.3	-11.1
NbN90-GO10	5900	4.0	-11.7
NbN55-GO45	8000	4.6	-23.0
NbN25-GO75	2200	2.4	-16.1
GO100	2100	2.3	-12.3

The rejection performances of PEG (Mw: 4000) as neutral molecules, an anionic dye and salts were further compared, as shown in Fig. 8. It was observed that the rejections of PEG (Mw: 4000) by NbN90-GO10 and NbN55-GO45 were lower than those by NbN100, NbN25-GO75 and GO100. However, it was interesting to observe that for all composite membranes, including NbN90-GO10 and NbN55-GO45, the EB rejection (molecular size of approximately 1.2 × 3.1 nm) was nearly 100%. Furthermore, the results for the rejection of salt were similar (Fig. 8b). The trend of a higher rejection of Na_2SO_4 with a higher weight ratio of GO in the range from 0 to 45 wt% could be observed and the NbN55-GO45 showed a higher rejection of Na_2SO_4 as compared with the other membranes. These rejection performances could be probably related to the membrane surface charge. The surface charge (ζ-potential) of the composite membranes were measured (Table 2). The NbN100 had a negative surface charge because of the nature of the niobate crystal structure [18]. It was observed that the potential of the composite membranes was more negative as compared with NbN100. Among the composite membranes, the NbN55-GO45 showed the most negative surface charge of −23.0 mV. This

negative surface charge arose from the existence of GO nanosheets with the potential of GO from −30 to −40 mV [15] at the surface of the composite membrane. The relatively low degree of negative charge of GO100 (−12 mV) shown in Table 2 arose from the shielding effect of TEOA on the surface of GO [30]. Based on the results of the surface ζ-potential, it was assumed that the negatively charged surface of NbN-GO composite membranes enhanced the rejection of multivalent anions owing to the Donnan exclusion mechanism [41,42], while the effect of surface ζ-potential was small for the rejection of monovalent anions. The stability of the membranes was also evaluated by immersion test in water with stirring for 12 hours and long-term measurement of membrane performances. For GO membrane fabricated by vacuum filtration without any chemical binders, some parts of the membrane surface were apparently peeled off from the support. In contrast, stable membrane surfaces were observed for NbN55-GO45 and NbN100 (Fig. S2). Furthermore, NbN55-GO45 showed stable water permeability of around 20 L m^{-2} h^{-1} bar^{-1} (Fig. S3) and EB rejection of around 98% for over 40 hours. Thus, the composite membrane, especially NbN55-GO45, exhibited superior water permeability and high structural stability with comparable NF performances to the NbN and GO membranes. The importance of these results has not been previously reported.

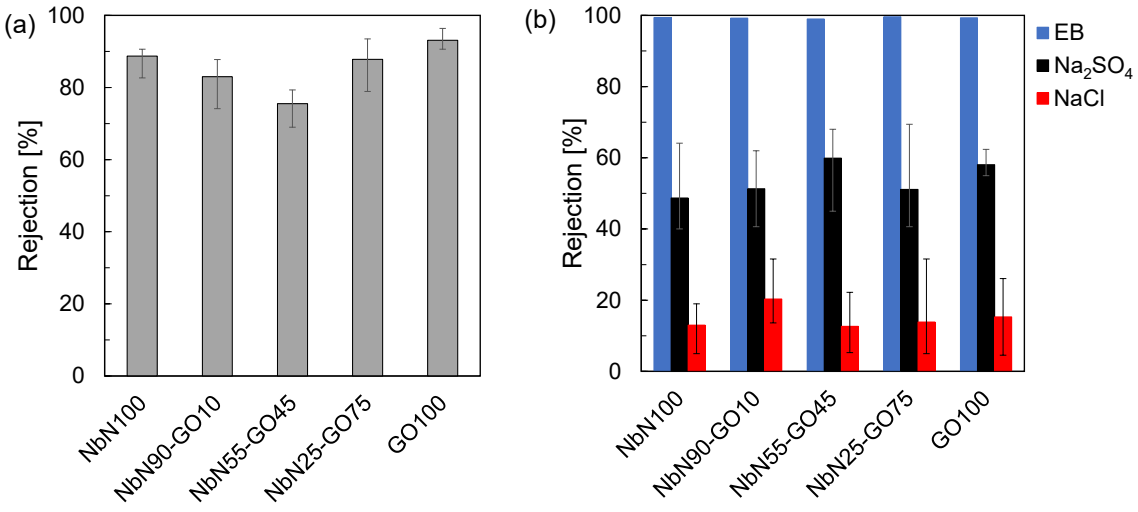

Fig. 8 Rejection of (a) PEG (Mw: 4000) and (b) EB, Na_2SO_4 and NaCl for NbN100, GO100 and NbN-GO composite membranes.

3.3 Discussion of channel structure of nanosheet composite membranes

Remarkable differences in the membrane structure and performances were observed by mixing the NbN and GO nanosheets for the fabrication of laminar nanosheet membranes. It was apparent that the composite ratio of NbN and GO strongly affected the structure and performances of the composite membranes. A schematic diagram of the channel structures for the composite membranes is shown in Fig. 9. In the laminar GO membranes, water molecules could pass through the 2D channels between GO nanosheets (Fig. 9d). In contrast, in the laminar niobate nanosheet membranes, it has been presented that voids may form as nanochannels [18]. In this study, NbN100 possessed a relatively larger channel size (3.3 nm estimated from MWCO) than GO100 (2.3 nm) and a stable structure in the wet condition. Considering that the niobate nanosheet thickness was 0.9 nm [31] and the interlayer spacing was 1.1 nm (wet condition), the free spacing between nanosheets was estimated to be only 0.2

nm. This free spacing hardly changed in the presence of water because of the dense structure cross-linked by TEOA, which prevented water from entering the interlayers. Instead, the water molecules could pass through the inter-nanosheet void structure (Fig. 9a). It has been reported that the presence of non-idealities, such as pinhole defects in the interiors of GO nanosheet, voids and disordered micro-structure derived from relatively random stacking in the laminar GO membranes, strongly affect the water permeability [43,44]. Seen from this perspective, one may propose that the laminar niobate nanosheet membranes are likely to possess a non-ideal structure by considering the small lateral sheet size and the dense structure which block water permeation. However, despite the expectation of short water pathway, NbN100 showed lower water permeability than GO100 (Fig. 6). It is assumed that the low water permeability is due to the membrane structure with a low porosity and/or less-connected nanochannels for NbN100 with a membrane thickness of 45 nm.

In the NbN-GO composite membranes, as can be seen from results of the characterization and membrane performances, the membrane structure could be classified as follows: NbN-based channel structure (NbN90-GO10 and NbN55-GO45) and GO-based channel structure (NbN25-GO75). The NbN-rich membranes had a highly stable structure in the wet condition and relatively large nanochannels. This suggested that the NbN-rich membranes had similar nanochannels derived from a void structure as NbN100. We attributed the formation of the larger nanochannels to the loose stacking structure of the void by mixing with a low quantity of GO (Fig. 9b), which resulted in a membrane structure with a high porosity and high water permeability for NbN55-GO45. Therefore, NbN55-GO45

was considered to possess an NbN-based channel structure in spite of the slightly larger volume of GO than NbN. In contrast, in the GO-rich membrane (NbN25-GO75), swelling of the laminar structure was observed but small nanochannels (2.4 nm) were formed. Thus, we assumed that NbN25-GO75 mainly had interlayer nanochannels between the GO nanosheets and included the smaller sized NbN in the interlayer (Fig. 9c).

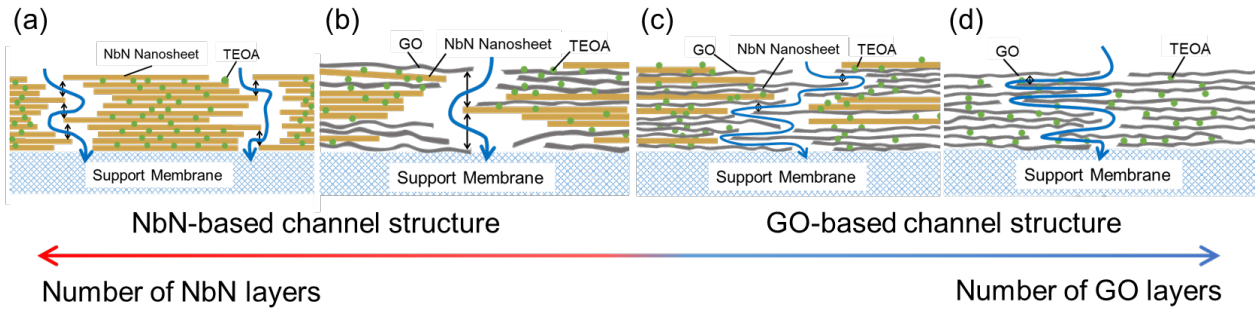

Fig. 9 Schematic diagram of channel structures in NbN-GO composite membranes.

Finally, Table 3 compares the membrane performances of the NbN-GO composite membranes, recent various GO membranes and commercialized NF polymer membranes. The NbN-GO composite membranes showed relatively higher water permeability while maintaining a similar salt rejection ability compared with the reported GO membranes, although surface modified GO membranes with excellent water permeability and salt rejection have recently reported [7]. Further improvement in the membrane performance of NbN-GO composite membranes would be expected by optimizing the membrane thickness or different composite patterns in the near future.

Table 3. Comparison of membrane performance of NbN-GO composite membranes with those of various GO membranes and some commercial NF membranes.

Membrane (nanosheet/support)	Fabrication Method	Permeability (L/m^2 h bar)	Rejection (%) NaCl	Na_2SO_4	ref
NbN100/CN	Vacuum filtration	2.9	13.0	48.7	This work
NbN55-GO45/CN	Vacuum filtration	20.2	12.7	59.9	This work
NbN25-GO75/CN	Vacuum filtration	9.5	13.9	51.1	This work
GO/PAN nanofibrous mat	Vacuum filtration	1.8	9.8	56.7	[11]
GO-PDA/PSf	Vacuum filtration	18.5	4	28	[45]
GO/PSf	Pressurized filtration	11	25	65	[12]
GO-PSS/PAN	Pressurized filtration	16.8	-	97.1	[7]
GO-TiO_2-PSS/PAN	Pressurized filtration	56.8	-	93.9	[7]
GO-TMC/PDA-PSf	Layer-by-layer	30	29	26	[8]
GO-MWCNT/PVDF	Vacuum filtration	11.3	39.7	81.0	[32]
GO-MoS_2/PVDF	Pressurized filtration	10.2	43.2	65.2	[33]
NTR-7450 (Nitto Denko)	-	9.2	51	92	[46]
NTR-7410 (Nitto Denko)	-	50	15	55	[46]
DK (SUEZ)	-	7.3	-	93	[7]

CN: cellulose nitrate, PAN: polyacrylonitrile, PDA: polydopamine, PSf: polysulfone, PSS: polystyrene sulfonate, TMC: 1,3,5-benzene tricarbonyltrichloride, MWCNT: multi-walled carbon nanotube, PVDF: polyvinylidene fluoride

4. Conclusions

NbN-GO nanosheet composite membranes with different composite ratios were successfully fabricated by vacuum filtration. The membrane structure could be classified according to the composite ratio, that is, an NbN-based channel structure and a GO-based channel structure. The NbN-rich membranes had a more stable structure in the wet condition and a membrane structure with larger channel size as compared with the GO-rich membranes. NbN55-GO45 showed high water permeability and excellent rejection against an organic dye and salts. A lower PEG rejection but slightly higher salt rejection were observed for NbN55-GO45 than for NbN100 and GO100 because of the formation of larger sized channels and the more negative surface in NbN55-GO45. Therefore, NbN55-GO45 can be considered to possess an NbN-based channel structure in spite of the slightly larger volume of GO than NbN.

Owing to the unique surface properties of metal oxide nanosheets, such as photocatalytic activity and surface acidity, these nanosheet composite membranes could be applied in a catalytic membrane reactor. Furthermore, organic solvent filtration has recently been a targeted application for 2D nanosheet membranes owing to their good solvent resistance. It is thus believed that NbN-GO composite membranes may have great potential for various practical applications.

Acknowledgments

This work was supported by JSPS KAKENHI Grant Number 19K05121 and Sumitomo Electric,

SEI Group CSR Foundation 2017.

References

[1] G. Liu, W. Jin, N. Xu, Two-Dimensional-Material Membranes: A New Family of High-Performance Separation Membranes, Angew. Chemie Int. Ed. 55 (2016) 13384–13397. doi:10.1002/anie.201600438.

[2] S. Dervin, D.D. Dionysiou, S.C. Pillai, 2D nanostructures for water purification: graphene and beyond, Nanoscale. 8 (2016) 15115–15131. doi:10.1039/C6NR04508A.

[3] Y. Kang, Y. Xia, H. Wang, X. Zhang, 2D Laminar Membranes for Selective Water and Ion Transport, Adv. Funct. Mater. 1902014 (2019) 1–17. doi:10.1002/adfm.201902014.

[4] G. Liu, W. Jin, N. Xu, Graphene-based membranes, Chem. Soc. Rev. 44 (2015) 5016–5030. doi:10.1039/C4CS00423J.

[5] H. Huang, Z. Song, N. Wei, L. Shi, Y. Mao, Y. Ying, L. Sun, Z. Xu, X. Peng, Ultrafast viscous water flow through nanostrand-channelled graphene oxide membranes, Nat. Commun. 4 (2013) 2979–2987. doi:10.1038/ncomms3979.

[6] M. Hu, Z. Cui, J. Li, L. Zhang, Y. Mo, D.S. Dlamini, H. Wang, B. He, J. Li, H. Matsuyama, Ultra-low graphene oxide loading for water permeability, antifouling and antibacterial improvement of polyethersulfone/sulfonated polysulfone ultrafiltration membranes, J. Colloid Interface Sci. 552 (2019) 319–331. doi:10.1016/j.jcis.2019.05.065.

[7] M. Zhang, K. Guan, Y. Ji, G. Liu, W. Jin, N. Xu, Controllable ion transport by surface-charged graphene oxide membrane, Nat. Commun. 10 (2019) 1–8. doi:10.1038/s41467-019-09286-8.

[8] M. Hu, B. Mi, Enabling Graphene Oxide Nanosheets as Water Separation Membranes, Environ. Sci. Technol. 47 (2013) 3715–3723. doi:10.1021/es400571g.

[9] W.S. Hung, C.H. Tsou, M. De Guzman, Q.F. An, Y.L. Liu, Y.M. Zhang, C.C. Hu, K.R. Lee, J.Y. Lai, Cross-linking with diamine monomers to prepare composite graphene oxide-framework membranes with varying d-spacing, Chem. Mater. 26 (2014) 2983–2990. doi:10.1021/cm5007873.

[10] W. Wang, E. Eftekhari, G. Zhu, X. Zhang, Z. Yan, Q. Li, Graphene oxide membranes with tunable permeability due to embedded carbon dots, Chem. Commun. 50 (2014) 13089–13092. doi:10.1039/c4cc05295a.

[11] J. Wang, P. Zhang, B. Liang, Y. Liu, T. Xu, L. Wang, B. Cao, K. Pan, Graphene Oxide as an Effective Barrier on a Porous Nanofibrous Membrane for Water Treatment, ACS Appl. Mater. Interfaces. 8 (2016) 6211–6218. doi:10.1021/acsami.5b12723.

[12] Y. Wei, Y. Zhang, X. Gao, Y. Yuan, B. Su, C. Gao, Declining flux and narrowing

nanochannels under wrinkles of compacted graphene oxide nanofiltration membranes, Carbon N. Y. 108 (2016) 568–575. doi:10.1016/j.carbon.2016.07.056.

[13] H.B. Park, J. Kamcev, L.M. Robeson, M. Elimelech, B.D. Freeman, Maximizing the right stuff: The trade-off between membrane permeability and selectivity, Science (80-.). 356 (2017) 1138–1148. doi:10.1126/science.aab0530.

[14] Y.H. Cho, H.W. Kim, H.D. Lee, J.E. Shin, B.M. Yoo, H.B. Park, Water and ion sorption, diffusion, and transport in graphene oxide membranes revisited, J. Memb. Sci. 544 (2017) 425–435. doi:10.1016/j.memsci.2017.09.043.

[15] H. Shen, N. Wang, K. Ma, L. Wang, G. Chen, S. Ji, Tuning inter-layer spacing of graphene oxide laminates with solvent green to enhance its nanofiltration performance, J. Memb. Sci. 527 (2017) 43–50. doi:10.1016/j.memsci.2017.01.003.

[16] Z.X. Low, J. Ji, D. Blumenstock, Y.M. Chew, D. Wolverson, D. Mattia, Fouling resistant 2D boron nitride nanosheet – PES nanofiltration membranes, J. Memb. Sci. 563 (2018) 949–956. doi:10.1016/j.memsci.2018.07.003.

[17] P. Sun, Q. Chen, X. Li, H. Liu, K. Wang, M. Zhong, J. Wei, D. Wu, R. Ma, T. Sasaki, H. Zhu, Highly efficient quasi-static water desalination using monolayer graphene oxide/titania hybrid laminates, NPG Asia Mater. 7 (2015) e162. doi:10.1038/am.2015.7.

[18] K. Nakagawa, H. Yamashita, D. Saeki, T. Yoshioka, T. Shintani, E. Kamio, H.T. Kreissl, S.C.E. Tsang, S. Sugiyama, H. Matsuyama, Niobate nanosheet membranes with enhanced stability for nanofiltration, Chem. Commun. 53 (2017) 7929–7932. doi:10.1039/C7CC03911E.

[19] K. Nakagawa, T. Sera, M. Kunimatsu, H. Yamashita, T. Yoshioka, T. Shintani, E. Kamio, S.C.E. Tsang, H. Matsuyama, Two-dimensional niobate nanosheet membranes for water treatment: Effect of nanosheet preparation method on membrane performance, Sep. Purif. Technol. 219 (2019) 222–229. doi:10.1016/j.seppur.2019.03.031.

[20] L. Sun, H. Huang, X. Peng, Laminar MoS2 membranes for molecule separation, Chem. Commun. 49 (2013) 10718–10720. doi:10.1039/c3cc46136j.

[21] Z. Wang, Q. Tu, S. Zheng, J.J. Urban, S. Li, B. Mi, Understanding the Aqueous Stability and Filtration Capability of MoS2 Membranes, Nano Lett. 17 (2017) 7289–7298. doi:10.1021/acs.nanolett.7b02804.

[22] G. Liu, J. Shen, Q. Liu, G. Liu, J. Xiong, J. Yang, W. Jin, Ultrathin two-dimensional MXene membrane for pervaporation desalination, J. Memb. Sci. 548 (2018) 548–558. doi:10.1016/j.memsci.2017.11.065.

[23] K. Varoon, X. Zhang, B. Elyassi, D.D. Brewer, M. Gettel, S. Kumar, J.A. Lee, S. Maheshwari, A. Mittal, C.-Y. Sung, M. Cococcioni, L.F. Francis, A. V. McCormick, K.A. Mkhoyan, M. Tsapatsis, Dispersible Exfoliated Zeolite Nanosheets and Their Application as a Selective Membrane, Science (80-.). 334 (2011) 72–75. doi:10.1126/science.1208891.

[24] T. Rodenas, I. Luz, G. Prieto, B. Seoane, H. Miro, A. Corma, F. Kapteijn, F.X. Llabrés i

Xamena, J. Gascon, Metal–organic framework nanosheets in polymer composite materials for gas separation, Nat. Mater. 14 (2015) 48–55. doi:10.1038/nmat4113.

[25] G. Li, K. Zhang, T. Tsuru, Two-Dimensional Covalent Organic Framework (COF) Membranes Fabricated via the Assembly of Exfoliated COF Nanosheets, ACS Appl. Mater. Interfaces. 9 (2017) 8433–8436. doi:10.1021/acsami.6b15752.

[26] D.R. Dreyer, S. Park, C.W. Bielawski, R.S. Ruoff, The chemistry of graphene oxide, Chem. Soc. Rev. 39 (2010) 228–240. doi:10.1039/B917103G.

[27] S. Stankovich, D.A. Dikin, R.D. Piner, K.A. Kohlhaas, A. Kleinhammes, Y. Jia, Y. Wu, S.T. Nguyen, R.S. Ruoff, Synthesis of graphene-based nanosheets via chemical reduction of exfoliated graphite oxide, Carbon N. Y. 45 (2007) 1558–1565. doi:10.1016/j.carbon.2007.02.034.

[28] S. Zheng, Q. Tu, J.J. Urban, S. Li, B. Mi, Swelling of Graphene Oxide Membranes in Aqueous Solution: Characterization of Interlayer Spacing and Insight into Water Transport Mechanisms, ACS Nano. 11 (2017) 6440–6450. doi:10.1021/acsnano.7b02999.

[29] E. Yang, M.H. Ham, H.B. Park, C.M. Kim, J. ho Song, I.S. Kim, Tunable semi-permeability of graphene-based membranes by adjusting reduction degree of laminar graphene oxide layer, J. Memb. Sci. 547 (2018) 73–79. doi:10.1016/j.memsci.2017.10.039.

[30] G. Liu, K. Han, H. Ye, C. Zhu, Y. Gao, Y. Liu, Y. Zhou, Graphene oxide/triethanolamine modified titanate nanowires as photocatalytic membrane for water treatment, Chem. Eng. J. 320 (2017) 74–80. doi:10.1016/j.cej.2017.03.024.

[31] K. Nakagawa, T. Jia, W. Zheng, S.M. Fairclough, M. Katoh, S. Sugiyama, S.C. Edman Tsang, Enhanced photocatalytic hydrogen evolution from water by niobate single molecular sheets and ensembles, Chem. Commun. 50 (2014) 13702–13705. doi:10.1039/C4CC04726E.

[32] Y. Han, Y. Jiang, C. Gao, High-Flux Graphene Oxide Nanofiltration Membrane Intercalated by Carbon Nanotubes, ACS Appl. Mater. Interfaces. 7 (2015) 8147–8155. doi:10.1021/acsami.5b00986.

[33] P. Zhang, J.L. Gong, G.M. Zeng, B. Song, W.C. Cao, H.Y. Liu, S.Y. Huan, P. Peng, Novel “loose” GO/MoS2 composites membranes with enhanced permeability for effective salts and dyes rejection at low pressure, J. Memb. Sci. 574 (2019) 112–123. doi:10.1016/j.memsci.2018.12.046.

[34] W.H. Jr, R. Offeman, Preparation of graphitic oxide, J. Am. Chem. Soc. 80 (1958) 1339. http://pubs.acs.org/doi/pdf/10.1021/ja01539a017 (accessed February 3, 2014).

[35] D.C. Marcano, D. V. Kosynkin, J.M. Berlin, A. Sinitskii, Z. Sun, A. Slesarev, L.B. Alemany, W. Lu, J.M. Tour, Improved Synthesis of Graphene Oxide, ACS Nano. 4 (2010) 4806–4814. doi:10.1021/nn1006368.

[36] K. Nakagawa, S. Araya, M. Kunimatsu, T. Yoshioka, T. Shintani, E. Kamio, H. Matsuyama, Fabrication of Stacked Graphene Oxide Nanosheet Membranes Using Triethanolamine as a Crosslinker and Mild Reducing Agent for Water Treatment, Membranes (Basel). 8 (2018)

130. doi:10.3390/membranes8040130.
[37] C.-N. Yeh, K. Raidongia, J. Shao, Q.-H. Yang, J. Huang, On the origin of the stability of graphene oxide membranes in water, Nat. Chem. 7 (2015) 166–170. doi:10.1038/nchem.2145.
[38] H.T. Kreissl, K. Nakagawa, Y.-K. Peng, Y. Koito, J. Zheng, S.C.E. Tsang, Niobium oxides: Correlation of acidity with structure and catalytic performance in sucrose conversion to 5-hydroxymethylfurfural, J. Catal. 338 (2016) 329–339. doi:10.1016/j.jcat.2016.03.007.
[39] H.T. Kreissl, M.M.J. Li, Y.-K. Peng, K. Nakagawa, T.J.N. Hooper, J. V. Hanna, A. Shepherd, T.-S. Wu, Y.-L. Soo, S.C.E. Tsang, Structural Studies of Bulk to Nanosize Niobium Oxides with Correlation to Their Acidity, J. Am. Chem. Soc. 139 (2017) 12670–12680. doi:10.1021/jacs.7b06856.
[40] C.M. Tam, A.Y. Tremblay, Membrane pore characterization—comparison between single and multicomponent solute probe techniques, J. Memb. Sci. 57 (1991) 271–287. doi:10.1016/S0376-7388(00)80683-3.
[41] T. Tsuru, D. Hironaka, T. Yoshioka, M. Asaeda, Titania membranes for liquid phase separation: effect of surface charge on flux, Sep. Purif. Technol. 25 (2001) 307–314. doi:10.1016/S1383-5866(01)00057-0.
[42] N. Hilal, H. Al-Zoubi, N.A. Darwish, A.W. Mohamma, M. Abu Arabi, A comprehensive review of nanofiltration membranes:Treatment, pretreatment, modelling, and atomic force microscopy, Desalination. 170 (2004) 281–308. doi:10.1016/j.desal.2004.01.007.
[43] V. Saraswat, R.M. Jacobberger, J.S. Ostrander, C.L. Hummell, A.J. Way, J. Wang, M.T. Zanni, M.S. Arnold, Invariance of water permeance through size-differentiated graphene oxide laminates, ACS Nano. 12 (2018) 7855–7865. doi:10.1021/acsnano.8b02015.
[44] A. Gogoi, A. Koneru, K. Anki Reddy, Effect of graphene oxide (GO) nanosheet sizes, pinhole defects and non-ideal lamellar stacking on the performance of layered GO membranes: an atomistic investigation, Nanoscale Adv. (2019). doi:10.1039/c9na00235a.
[45] Y. Xu, M. Wu, S. Yu, Y. Zhao, C. Gao, J. Shen, Ultrathin and stable graphene oxide fi lm via intercalation polymerization of polydopamine for preparation of digital inkjet printing dye, J. Memb. Sci. 586 (2019) 15–22. doi:10.1016/j.memsci.2019.05.057.
[46] W. Zhang, G. He, P. Gao, G. Chen, Development and characterization of composite nanofiltration membranes and their application in concentration of antibiotics, Sep. Purif. Technol. 30 (2003) 27–35. doi:10.1016/S1383-5866(02)00095-3.